A hydrodynamic study of a floating circular OWC

R. K. Sykes[1], A.W. Lewis[2] and G.P. Thomas[3]

[1] Garrad Hassan and Partners,
St Vincent's Works, Silverthorne Lane, Bristol, UK
E-mail: Rebecca.Sykes@garradhassan.com

[2] Hydraulics and Maritime Research Centre, University College Cork,
Cork, Ireland

[3] Department of Applied Mathematics, University College Cork,
Cork, Ireland

Abstract

The development path of a wave energy device from concept to full-scale device is comprised typically of a numerical study and experimental modelling at a number of scales. Numerical models based upon Boundary Element Method (BEM) codes are widely used within the offshore industry and have been validated for fixed Oscillating Water Column (OWC) devices of shoreline type, providing confidence in their use. However, as OWC technology develops and devices are designed for offshore environments, validation of numerical codes for floating OWCs is required. In comparison with characteristic offshore structure design, which aims to minimise motion, wave energy device design has the goal of energy extraction. This may require significant motion, balanced by the power take-off mechanism, and therefore necessitating additional validation for the purpose.

The aim of this paper is to provide a preliminary assessment of the validity of employing a BEM code to predict the displacement and associated hydrodynamic properties of a simple floating undamped OWC in the form of a hollow vertical circular cylinder. Predictions obtained from the WAMIT code are compared with experimental measurements at selected frequencies and with increasing wave amplitude. An investigation of the agreement for predicted and measured pressures is also undertaken.

Keywords: Floating OWC, numerical modelling, experimental modelling, vertical cylinder.

Nomenclature

A	Hydrodynamic added mass matrix
B	Hydrodynamic damping matrix
C	Hydrostatic stiffness matrix
$\mathbb{X}$	Excitation force
L	Linearised quantity
T	Wave period
M	Mechanical mass matrix
NU	Circumferential discretisation parameter
NV	Radial discretisation parameter for horizontal patches or vertical discretisation for vertical patches
O	Coordinate system origin
P	Dynamic pressure
R	Rotation matrix
a	Incident wave amplitude
d	Draft
g	Acceleration due to gravity
h	Water depth
i	Unit complex number
k	Wavenumber
n	Normal
r	Radius
t	Time
x, y, z	Cartesian coordinates
Φ	Harmonic velocity potential
η	Free surface elevation
v	Body surface position
ρ	Density
φ	Velocity potential
ω	Wave frequency
ξ	Body displacement

Subscripts

B	Body
D	Diffracted
I	Incident
INT	Intermediary
R	Radiated
S	Scattered
i	Inner
o	Outer
1	Surge
2	Heave
3	Pitch
4	Roll
5	Pitch
6	Yaw

1 Introduction

The development of wave energy devices should consider all aspects of the transfer of energy from wave to wire. The hydrodynamic relationship between the device and the waves, being the first step of this transfer and a primary concern, needs to be well considered in any modelling exercise. Hydrodynamic

© Proceedings of the 8th European Wave and Tidal Energy Conference, Uppsala, Sweden, 2009

analysis continues to be best met through the combined use of numerical modelling and experimental testing, with the latter being used when the assumptions underpinning the numerical techniques are not met. Most of the available numerical techniques are based upon linear hydrodynamic theory and are limited by assumptions of small wave amplitude, hence the necessity of experimental modelling for the understanding of non-linear processes such as extreme wave interaction. However, the linear regime is of great interest, since accurate estimates of power production will be most important in the sea states with the most energy over time, which will typically be moderate in size.

It is important for the progress of wave energy that the balance of benefits obtained from co-ordinated numerical and experimental work is well-understood, to allow the timely use of resources appropriately for maximum technological gain. The use of wave tanks is expensive and device developers who have conducted experimental testing are generally reluctant to release results, due to commercial sensitivities, and so there is limited evidence on which to base developmental decisions.

The OWC wave energy device has been studied, developed and prototyped for mainly fixed systems. Validation work has been carried out for linear hydrodynamic models based on BEM codes but this has not yet been extended to floating OWC. For the circular OWC of interest herein, Sykes, Lewis & Thomas [1] demonstrated good agreement between measured pressures and those predicted by the BEM code WAMIT, within the limitations of linear theory, for a fixed device. Of particular interest was the experimental identification of a point of zero hydrodynamic pressure within the cylinder. This work was extended in [2] to a floating form of the same configuration, stiffly-moored by springs, but such good agreement was not found in that case, suggesting significant differences between the fixed and floating OWCs.

The hydrodynamic-aerodynamic coupling in an OWC chamber dictates that the pressure at the internal water surface changes continuously under operational conditions, being related to the flow through the turbine, and may be significantly different to the external ambient value. However, the internal water surface is unconstrained in the present set of experiments and thus the internal and external surface pressures are the same. As such there are obvious geometric similarities between the circular OWC and a circular moonpool, which is a vertical well used within ships for drilling or diving operations. Large motions can occur within the moonpool when station-keeping and in a seaway and work is ongoing to maximise the operational range of conditions by minimizing the motions within the moonpool. Minimising the oscillation is of course the opposite aim to the wave energy application.

Aalbers [3] considered a circular cylindrical moonpool in a square profile ship section and constructed a mathematical model by assigning the water column as an additional degree of freedom and derived the hydrodynamic coefficients experimentally. It was concluded that the quadratic damping coefficient, included in the model, does not scale accordingly to the usual Froude law and must be determined empirically. Knott & Flower [4] had previously shown that the size of vortices formed at inflow and outflow from a pipe exit could be as large as the diameter of the pipe. In reference to this work, Aalbers concluded that a 100mm pipe would generate vortices from opposite points on the pipe wall and that these vortices would interact strongly, so hindering their development and reducing the vortex damping; it was speculated that this effect would increase with diameter as the vortices are allowed to form fully.

A variation in vortex shedding was highlighted in work by Fung [5], also using experimental methods to determine added mass and damping coefficients on fixed circular moonpools. It was found that the combined damping (linear and quadratic) was greater on the down-stroke of the water column than on the up-stroke. This discrepancy was attributed to vortex formation and was found to increase with the amplitude of oscillation for the down-stroke but not the up-stroke. In addition, it was observed that the mean elevation of the free surface inside the moonpool increased for low wave frequencies; Fung claimed that this was an advantage for wave energy devices but no reasoning was presented to support this assertion. However, the possible analogy between circular OWCs and moonpools was identified.

Sphaier *et al.* [6] conducted an experimental study in an attempt to determine the optimal entrance geometry of the moonpool, with their target being to minimize the vertical water motion in the moonpool when waves are present. They measured the body and free surface motion in experimental tests of a vertical circular cylinder with moonpool, a similar geometry to that employed in the present paper, with varying sizes of orifice plate at the mouth of the water column. It was found that two resonant periods exist for the heave motion of the body and correspondingly similar double peak was seen in the relative motion of the water column. Progressively reducing the size of the orifice reduced the water column motion relative to the body; the wave period of maximum relative oscillations converged to a single resonant period, equal to that of correspondingly converged period of maximum oscillation for the body motion under the same narrowing orifice.

The results of [3], [5], [6] and work subsequent indicates that there may be a need for improved numerical models with the inclusion of viscosity, vortex shedding and nonlinear effects to provide an adequate description of the hydrodynamic behaviour within the moonpool. It is unclear how many of these requirements will need to be passed to the floating circular OWC but is important to acknowledge a potential need.

The purpose of this paper is to compare the numerical predictions, obtained from the linear hydrodynamic BEM code WAMIT, with the measurements from a dedicated experimental programme. Agreement would validate the use of a linear hydrodynamic BEM code for this particular geometry but a lack of agreement would expose the limitations of numerical modelling based on linear water wave theory.

The linear formulation of water wave theory is outlined in §2 and the numerical modelling considerations presented in §3. Details of the experimental programme are provided in §4. The measured body motions and pressures are presented in §5 and 6 respectively, with conclusions and further discussion in §7.

2 Theoretical and numerical formulation

Assuming the fluid to be incompressible and the motion irrotational enables the use of a velocity potential Φ , satisfying Laplace's equation

$$\frac{\partial^2\Phi}{\partial x^2}+\frac{\partial^2\Phi}{\partial y^2}+\frac{\partial^2\Phi}{\partial z^2}=0 \qquad (1)$$

in the fluid, with the velocity field given as $\underline{\nabla}\Phi$. The coordinates (x, y, z) form a right-handed system with the origin O in the mean water level, Ox horizontal in the direction of incident wave propagation, Oz vertically upwards and Oy horizontal completing the RHS system.

If the motion is driven by harmonic motion of radian frequency ω and within the linear wave regime, it is usual to separate the spatial and temporal dependence by writing

$$\Phi(x,y,z,t)=\mathrm{Re}\left\{\varphi(x,y,z)\,e^{-i\omega t}\right\} .$$

The reduced potential φ then satisfies Laplace's equation, together with the surface boundary condition

$$\frac{\partial^2\varphi}{\partial t^2}=-g\frac{\partial\varphi}{\partial z} \qquad (2)$$

on the mean free surface $z = 0$ and the bottom boundary condition

$$\frac{\partial\varphi}{\partial z}=0 \qquad (3)$$

on $z=-h$. Once the unknown potential φ has been determined, the free surface can be calculated from

$$\eta=-\frac{1}{g}\frac{\partial\Phi}{\partial t} \qquad (4)$$

evaluated on $z=0$. The dynamic pressure at any point in the fluid is then given by the linearised Bernoulli condition

$$P=-\rho\frac{\partial\Phi}{\partial t}=\mathrm{Re}\left\{-i\rho\omega\varphi\left(x,y,x\right)e^{-i\omega t}\right\} \qquad (5)$$

If a body is present, either fixed or undergoing small body motions, then the spatial potential is decomposed into

$$\varphi=\varphi_S+\varphi_R \qquad (6)$$

with the component potentials φ_S and φ_R associated with the scattered and radiated wavefields respectively and corresponding to a fixed and moving body. The determination of φ_S and φ_R is undertaken separately.

For the scattering problem, it is usual to employ a further decomposition and write

$$\varphi_S=\varphi_0+\varphi_D \qquad (7)$$

where φ_0 is the known incident wavefield given by

$$\varphi_0=-\frac{iga}{\omega}\frac{\cosh k\left(z+h\right)}{\cosh kh}e^{ikx} \qquad (8)$$

and φ_D is the unknown diffracted wavefield. The corresponding boundary condition of zero flux across the body boundary is

$$\frac{\partial\varphi_D}{\partial n}=-\frac{\partial\varphi_0}{\partial n}. \qquad (9)$$

The diffraction potential φ_D then satisfies (1), (2), (3), (9) and any requisite radiation conditions.

The corresponding radiation problem for φ_R utilises the decomposition

$$\varphi_R=\sum_{j=1}^{6}\left(-i\omega\xi_j\varphi_j\right) \qquad (10)$$

associated with the motion being composed of six independent body modes, where ξ_j is the complex amplitude of motion in the *j*-th mode. Each of the component potentials φ_i satisfies a further condition that defines the appropriate body motion and is given by

$$\begin{aligned}\frac{\partial\varphi_j}{\partial n}&=n_j \qquad & j=1,2,3\\ &=\left(\boldsymbol{r}\times\boldsymbol{n}\right)_j \qquad & j=4,5,6\end{aligned}\,. \qquad (11)$$

Thus each φ_i satisfies (1) – (3) together with the appropriate condition from (11), with j = 1,2,3 corresponding to the translational modes of surge, sway, heave and j = 4,5,6 corresponding to roll, pitch, yaw respectively.

Further details of the formulation, including the detailed boundary conditions can be obtained from Newman [7].

Analytic determination of the scattering and radiation potentials, φ_S and φ_j (j = 1,..,6), can only be achieved for a small number of simple shapes [7] and numerical determination is usually required. The numerical method of choice is the BEM, which is based upon a Green's function formulation and approximates the potential on the surface of the body using a distribution of sources or dipoles. There are a number of implementations of the BEM, including WAMIT, Aquadyn, AQWA, HYDROSTAR and WADAM.

It must be noted that the BEM codes do not calculate the motion amplitudes ξ_j directly, since these must satisfy an equation of motion and will be influenced by external forces such as those associated with mooring. Thus an equation of motion is required and it is necessary to determine the forces associated with the scattering and radiation potentials.

The force associated with the scattering potential is usually termed the exciting force, with the components of complex magnitude given by

$$\mathcal{X}_m = i\rho\omega \iint_{S_b} \varphi_S n_m \, \mathrm{d}S .$$

The radiation force is usually written as the sum of terms in phase with the body acceleration and velocity, defining the added mass and damping matrices

$$A_{mj} = \rho \iint_{S_b} \mathrm{Re}\, \varphi_j n_m \, \mathrm{d}S$$

$$B_{mj} = \rho\omega \iint_{S_b} \mathrm{Im}\, \varphi_j n_m \, \mathrm{d}S$$

Collecting all contributions gives the equation of motion as

$$\sum_{j=1}^{N} \left[-\omega^2 \left(M_{mj} + A_{mj} \right) + C_{mj} - i\omega B_{mj} \right] \xi_j = \mathcal{X}_m$$

for $m = 1,...,6$ to describe all translational and rotational modes. The additional terms in the equation are the mass matrix *M* and the hydrostatic stiff matrix *C*. If external forces, such as mooring forces, act on the body then these must be included in the equation of motion.

3 Implementation of the numerical model

Implementation of WAMIT requires the body surface to be discretised and the velocity potential (scattering and radiation) is calculated for each discrete panel. Errors can occur when an insufficient discretisation of the body leads to an inaccurate description of the flow [8].

The higher order method was used in this work, where the description of the body surface and velocity potential is given in terms of *b*-splines, rather than plane elements. These are defined for each section of the body known as a patch and *b*-splines potentially allow a more accurate characterisation of curved surfaces.

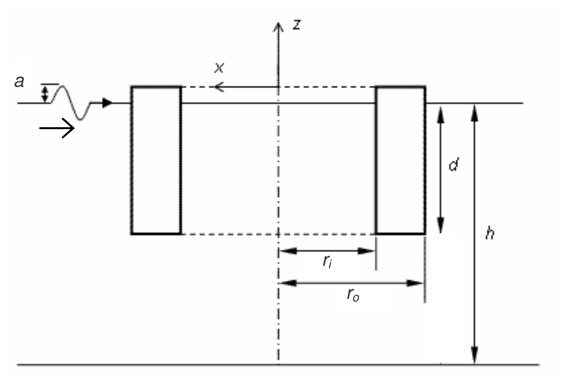

Figure 1. Cross section of OWC

A simplified OWC geometry, as shown in figure 1, was used for generic application. This required a thicker wall than the cylinder employed in [1] to enable sufficient instrumentation to be deployed. The vertical circular cylinder employed possessed an external radius r_o = 158mm, an internal radius r_i = 52mm and a nominal draft d = 300mm, with the water depth specified to be h = 1m.

The body was generated using four higher order patches, which were third order in the circumferential *NU* direction and fourth order in the *NV* direction, which is radial for horizontal patches or vertical for vertical patches. The orders of the inner and outer Gauss quadratures were set as advised by the WAMIT user manual [9] to be of one above the order and of the order of the *b*-splines respectively. The irregular frequency suppression tool was also utilised. A representation of the numerical model can be seen in figure 2, in which the component figures show the locations of the extents of the patches and the knots which control the *b*-spline.

4 Experimental testing

A model was fabricated for testing in the wave tank in the HMRC wave basin. The height of the model was 400mm and the ballast was determined to give a draft of 300mm, with other dimensions as associated with figure 1.

The wave basin in the HMRC measures 23.25m by 17.15m and the water depth was maintained at 1m. The wavemaker consists of forty bottom-hinged flap-type paddles with active absorption. The majority of the absorption occurs at the beach, which consists of a 5m length 1:10 inclined concrete sloping section, a 5m horizontal concrete plateaux with 2m length triangular wedge-shaped cages containing geotextile fabric positioned against the end wall.

The basin is fitted with a motion tracking system by Qualysis Medical AB based on three Proreflex infrared cameras, which can remotely determine the position of reflective markers with time. This system does not impinge on the motion of the model being tested and it was used to measure the global coordinates of three passive markers that were fixed to the model. The model was also instrumented with 10 pressure transducers. The pressure transducers used were Honeywell 176PC14HD2 and 176PC7HD2 low pressure differential transducers referenced to ambient air pressure. They were located within the structure of the model so as to record the pressure at the body surface at $x = -52$mm, $y = 0$mm, $z = -100$m, -140mm, -180mm, -220mm and -260mm. The relative displacement of the internal free surface was measured using a wave probe which was fixed rigidly to the model. Data sampling was taken at a rate of 32Hz for 256seconds.

The model was moored using a compliant slack mooring. Mooring forces were not included in the equation of motion, since such forces are considered negligible once steady state conditions have been established in the tank and the transient regime has been completed.

Each pressure transducer requires three electrical cables. The weight of the cables was supported using a compliant tether but due to the weight of the cabling required for the pressure transducers a slight list was induced in the attitude of the model such that the body coordinate system was rotated by ξ_4 = –0.38°, ξ_5 =

−2.76° and $\xi_6 = -0.16°$. The dimensions specified within this paper refer to this body coordinate system. This reflects the difficulties of testing at small scales and the significant improvements that have been achieved with the remote camera system for the purpose of motion measuring.

The model was tested in regular waves to enable a direct comparison to be made between experimental measurement and numerical prediction. Following specification of the incident wave periods and amplitudes, the tank was calibrated before the insertion of the model in the basin. The incident and reflected amplitudes were determined using the three probe method outlined by Isaacson [10] and a probe spacing of 0.2m and 0.4m was used. For the wave periods used in this work the resulting reflection coefficients ranged from 5.5% for the shortest waves to 14.7% for the longest ones. The details of the wave properties are given in table 1.

T [s]	a1 [mm]	a2 [mm]	a3 [mm]	a4 [mm]	a5 [mm]
1.03	5.1	10.1	15.1	19.9	24.9
1.14	5.5	11.2	16.8	22.3	27.6
1.18	5.7	11.3	17.0	22.4	27.8
1.28	6.4	12.6	18.6	24.4	30.0
1.39	6.1	12.2	18.3	24.2	29.9

Table 1: Wave parameters

5 Motion Response

The position coordinates of the reflective markers on the model enables the calculation of the rotation matrix, i.e. the matrix that maps the global coordinate system to the local one, at each sampled time step. The rotation matrix is unique and provides the rotational displacement of the model. Euler angles, being the angles of three coordinate rotations which make up any rotation, can be taken from the matrix. However, 12 possible sequences of rotation exist to give the total rotation, consequently the trio of angles derived by each sequence are not necessarily the same. The commonly-known Cardan angles have the sequence *x*, *y*, *z* whereas the convention in WAMIT is the sequence *z*, *y*, *x* [11, 12] giving the resulting rotation matrix,

$$R_{321}(\xi_6,\xi_5,\xi_4) = R_3(\xi_6)R_2(\xi_5)R_1(\xi_4)$$

$$= \begin{bmatrix} c_6c_5 & s_6c_4 + c_6s_5s_4 & s_6s_4 - c_6s_5c_4 \\ -s_6c_5 & c_6c_4 - s_6s_5s_4 & c_6s_4 + s_6s_5c_4 \\ s_5 & -s_4c_5 & c_4c_5 \end{bmatrix}$$

where $c_m = \cos\xi_m$ and $s_m = \sin\xi_m$ for $m = 4,5,6$.

As linear theory is employed, the rotation matrix can be linearised so that the sequence of rotations is not important and the rotation matrix is approximated by

$$L\{R_{321}(\xi_6,\xi_5,\xi_4)\} = \begin{bmatrix} 1 & \xi_6 & -\xi_5 \\ -\xi_6 & 1 & \xi_4 \\ \xi_5 & -\xi_4 & 1 \end{bmatrix}$$

If the body motion is considered linear, the above matrix will provide the rotational displacements. This should be the case when the experimental measurements are compared with numerical predictions based upon linear theory. However as the experimental programme did not assume linearity *a priori*, the non-linear matrix was used with little additional effort.

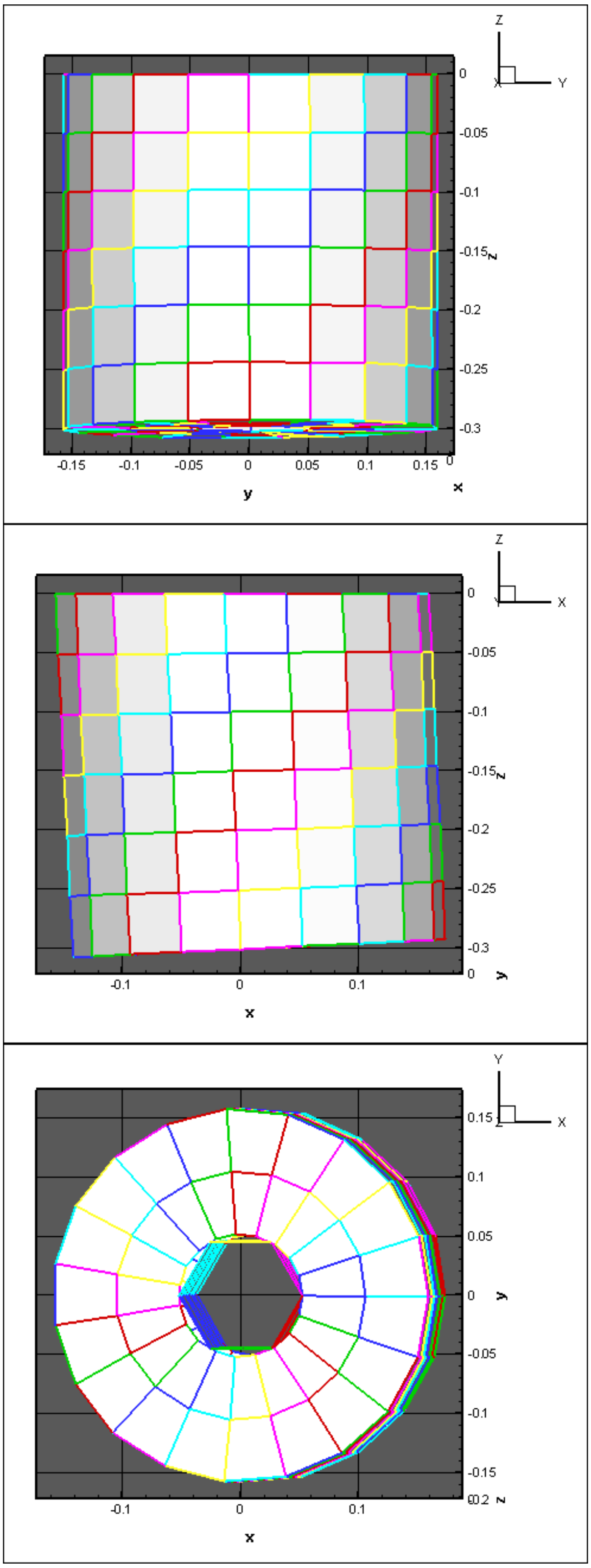

Figure 2: Representation of numerical model

The rotation matrix was created from the position coordinates at each time step by creating an intermediary coordinate system based on an orthogonal vector defined from the vectors given by the marker positions. The Euler angles were taken from the rotation matrix at each time step according to the z, y, x convention. The origin of the body coordinate system, necessary to define the translational motion was obtained using

$$O_B = O_{INT} - R^T O_{INTB}$$

where O_B is the body origin in the global frame, O_{INT} is the intermediary frame origin in the global frame and O_{INTB} is the vector of the intermediary frame origin in the body frame. A complete description for handling multiple frames of reference is contained in [13].

The calculated time series of the translations and rotations were analysed using the discrete Fourier transform (DFT) technique to obtain the first harmonic component. The numerical model predictions were made dimensional by employing the incident wave amplitude appropriate to that from the tank calibration. Figures 3, 4 and 5 show the comparisons between the experimental findings and numerical predictions for the surge, heave and pitch motions respectively, with the experimental findings based upon consideration of a time series comprised of approximately 200 wave periods.

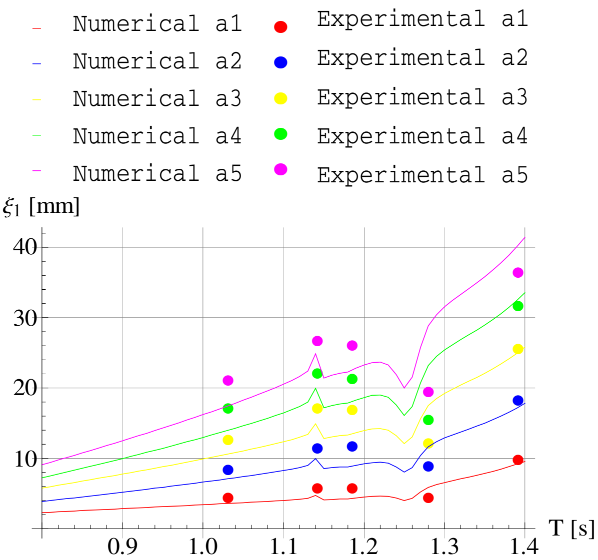

Figure 3: Surge motion of the model

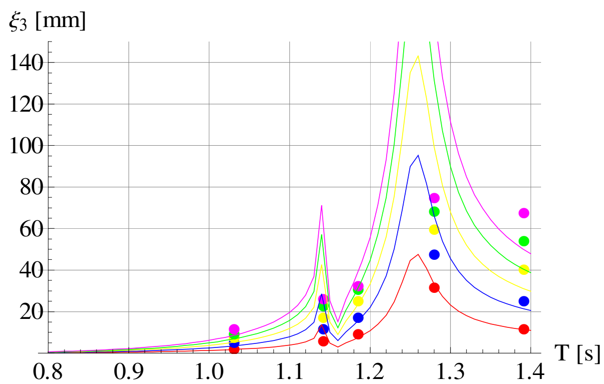

Figure 4: Heave motion of the model

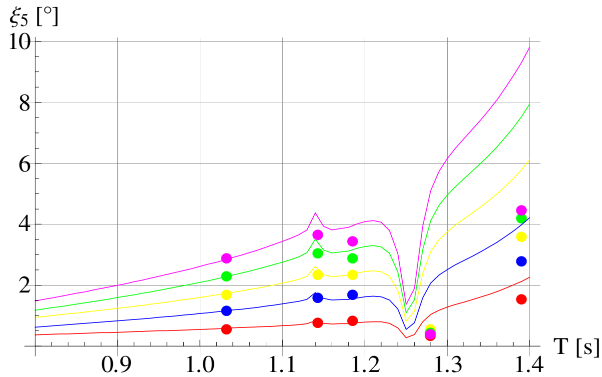

Figure 5: Pitch motion of the model

It would be expected from the limitations of linear wave theory that best agreement between prediction and experiment would be achieved for the smallest chosen wave amplitude at a given frequency. This is confirmed from the figures. With increasing amplitude, as would be expected, the agreement becomes poorer and the influence of nonlinearity and viscous damping is responsible for the failure to attain the resonant peaks predicted by the linear theory. This is more pronounced at certain frequencies, such as in pitch for $T = 1.39$s and at the heave resonance of $T = 1.28$s. As good agreement is generally present for the smallest waves, this suggests that linear theory could be considered as validated.

Figure 4 shows a double peak clearly in the heave response predicted by the numerical model, similar to that found by Sphaier *et al.* [6] and described earlier. This suggests that there are demonstrable analogies with the hydrodynamics of the circular moonpool but the strength of the analogy cannot be investigated further since [6] does not prove findings on surge or pitch motion.

It is interesting to note the large reduction in surge and pitch motion at the heave resonant period and this is due to the coupling between the modes, which is as a result of the listed attitude even though the listing is small. This reduction was clearly observable in experimental testing.

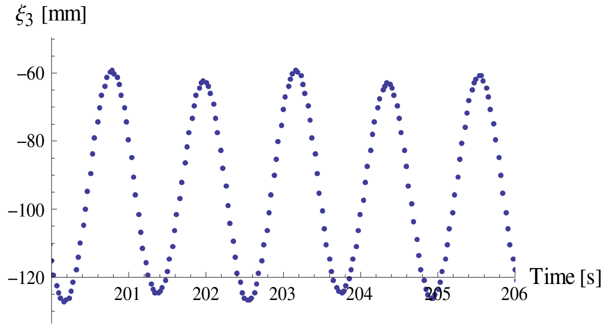

Figure 6: Heave motion of the model at $T = 1.18$s a = a5

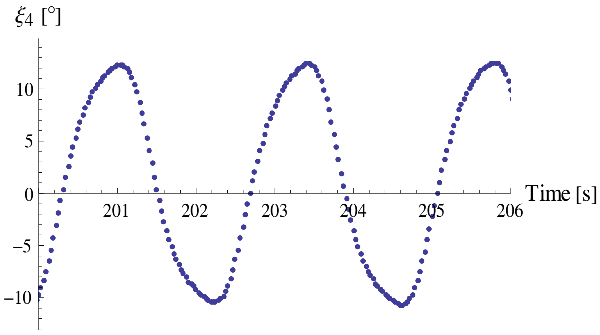

Figure 7: Roll motion of the model at $T = 1.18$s a = a5

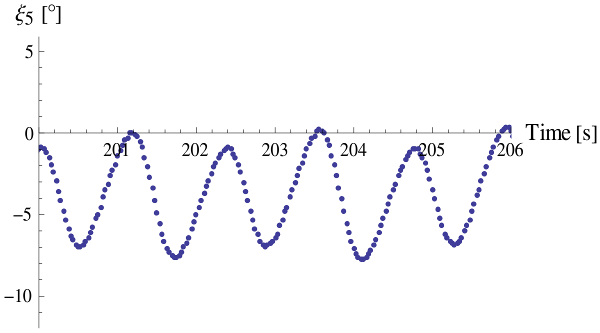

Figure 8: Pitch motion of the model at $T = 1.18$s a = a5

Time series were obtained for all six modes of motion. Considerations of symmetry suggested that amplitudes should be very small in sway, roll and yaw; this was generally the case and the resulting motions were of very small amplitude and usually occurring at the same frequency as the incident wave. Figures 6 – 8 show portions of the records at $T = 1.18$s for heave, roll and pitch at the largest incident amplitudes *a5*, as given in table 1; note that the roll motion was excited at a half of the forcing frequency, as were the sway and yaw motions. The heave (figure 6) and pitch (figure 8) series show the influence of nonlinearity and other mechanisms very clearly, whereas the equivalent records for smaller amplitudes are very uniform and repeatable. This was also observed at T = 1.14s and 1.28s for a5.

The roll and pitch motion also suffered intermittent periods of large unstable motions for a5, $T = 1.18$s and 1.28s covering approximately 30s intervals.

6 Pressure

The pressure was measured by the transducers and the water column free surface elevation by probe for a record of 256s. This was conducted under the same experimental conditions as employed in §5, using the incident amplitudes specified in table 1. A sample of the measured signals is given in figures 9 to 15, with duplicates where appropriate containing only selected pressure signals to illustrate specific features in greater detail. Those presented here are for the amplitude set *a1*. Although only two or three waves appear in the figures, dependent upon frequency, there is little variation in the record; this confirms consistency and good wave reproduction.

At the lowest wave period, $T = 1.03$s in figure 9, the phase of the relative position of the free surface just leads the pressures. All of the pressures are essentially in phase, with the magnitude being largest and smallest at the lowest ($z = -260$mm) and highest ($z = -100$mm) positions respectively and are exactly out of phase with the body motion.

At T = 1.14s, figure 10, the pressure at the highest position remains in phase with the relative free surface, while those lower down the column become progressively out of phase. The magnitude of the pressure is now greater at the top of the column than at the bottom. From figure 4, it is readily seen that the periods T = 1.03 and T = 1.14 lie on either side of the secondary heave resonance and this may be responsible for the differences in the pressure behaviour down the tube.

In figures 11 and 12, for $T = 1.18$s, the body motion, the relative water column motion and the highest pressure position are in phase. The pressure at the bottom is anti-phase to the surface values and those positions in between are attenuated and phase shifted by either signal dependant on their proximity to either end. This clearly indicates the influence of two anti-phased components, whose combined effect is to produce a zero dynamic pressure value at some point in the column between $z = -180$mm and $z = -220$mm; this can be compared with that observed in [1] though not necessarily for the same reasons. There is also some fluctuation observed in the extremes of lowest position pressure signal which may be associated with vortex shedding. This is more clearly shown in figure 12 where a repeating pattern can be observed.

The principal body heave resonance occurs at T = 1.28s and the relevant time series for this wave period are shown in figures 13 and 14. The body heave amplitude is significantly increased yet the relative water column motion has not increased appreciably from the previously examined wave period. The pressure at the bottom tapping remains out of phase with the body motion, as do the majority of the other positions. The pressure is reduced progressing up the column and the top position ($z = -100$mm) is no longer in phase with the relative water column motion. Although the pressure nearest to the free surface is not the largest, it is clearly seen that the signal is both repeatable and asymmetric; this non-linear behaviour could not be predicted by the linear numerical model and is possibly due to the differing effects of viscosity on the downward and upward motions of the flow.

At the longest wave period, T = 1.39s shown in figure 15, all pressure magnitudes are reduced. The pressures in the lower portion of the column continue to be out of phase with the heave motion and the heave motion and the relative water column motion are now almost in phase. There continues to be a reduction in the pressure progressing up the water column with a progressive phase shift towards that of the relative water column motion. The signal for the water column relative motion is noisy due to the measurement errors being a larger proportion of the signal for smaller amplitudes of the signal.

The experimental findings provide some agreement with the conclusion of Aalbers [3], regarding the heave motion and the relative water column motion being 180° out of phase at high frequency and in phase at low frequency. Progressing through the wave periods, shown in figures 9 to 15 indicates that the free surface just leads this relationship. This slight lead may be contributable to the pitch of the model causing some sloshing; pitch motion was not noted in [3].

The experimental results are only presented here in detail for the smallest amplitude *a1*, which would be expected to produce the best match with predictions employing linear wave theory. However, table 1 shows the range of amplitudes employed and it would be remiss not to make some comments upon the effect of increasing amplitude. At T = 1.14s, shown in figure 10 for *a1*, the flattening of the positive peak of the relative free surface becomes less distinct and the signal more sinusoidal with increasing amplitude. At T = 1.18s, figure 12 for *a1*, the lowest position becomes increasingly disturbed with fluctuations at the pressure minimums. The positions lower down the column are increasingly dominated with the phase of those at the top, such that their amplitudes are attenuated and phases shifted. For *a5*, the series at $z = -180$mm and $z = -220$mm are no longer symmetrical between each half of the cycle. Increasing the amplitude at T = 1.28s results in the phase shifting of the upper positions towards being in phase with the relative free surface throughout and asymmetry is observed between the positive and negative parts of the signals. Increased disturbance also occurs to both extremes of the pressure for the bottom position. The result of the phase shifting and amplitude attenuation suggests the existence of a system of multiple pressure signals, which do not scale equally with amplitude.

It had been previously found in [1] and [2] that the pressure took a zero value at some point in the column. This was not expressly sought in this case but examination of the record of the lowest tapping in figures 10 – 13 suggests that such a point, or points, do exist for the present scenario as well.

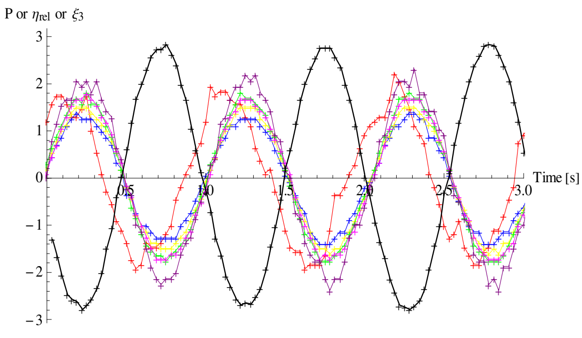

Figure 9: *P(t)*at pressure tappings and η_{rel}, T =1.03s

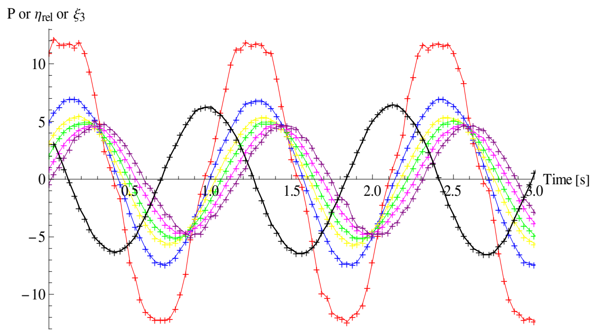

Figure 10 *P(t)* at pressure tappings and η_{rel}, T =1.14s

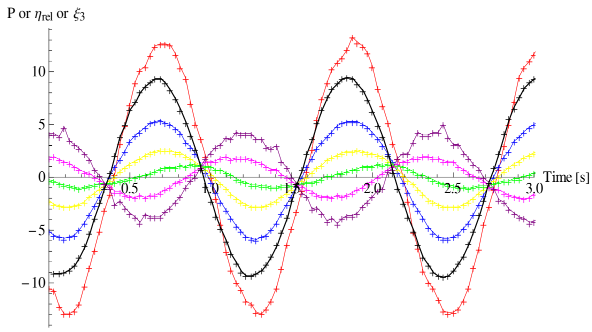

Figure 11: $P(t)$at pressure tappings and η_{rel}, T =1.18s

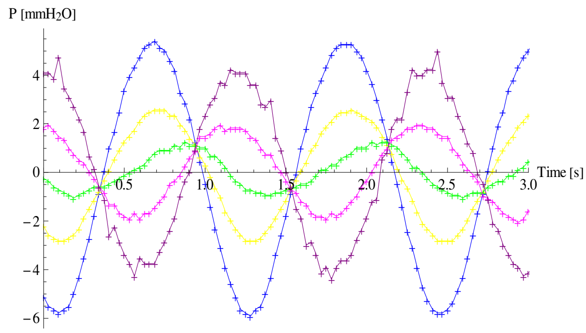

Figure 12: $P(t)$at pressure tappings only, T =1.18s

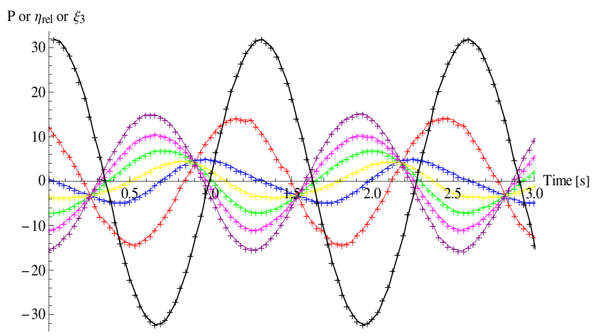

Figure 13: $P(t)$at pressure tappings and η_{rel}, T =1.28s

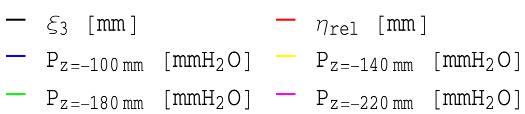

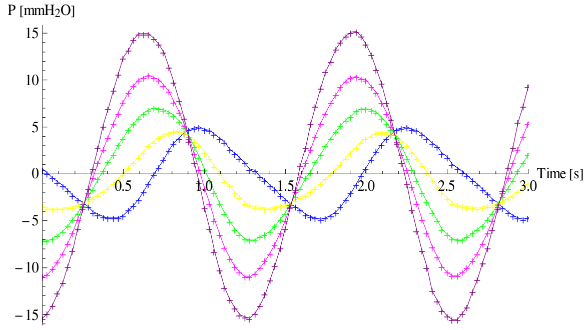

Figure 14: *P(t)*at pressure tappings only, T =1.28s

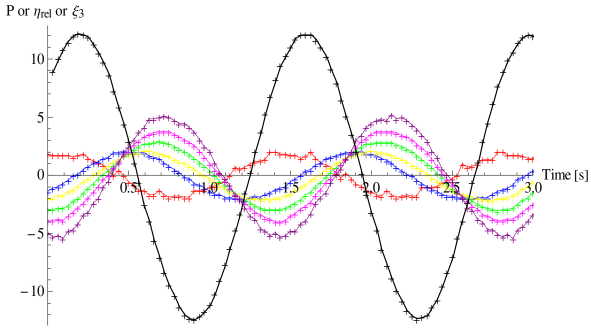

Figure 15: *P(t)* at pressure tappings and η_{rel}, T =1.39s

The complete time series for the pressures and the absolute motion of the water column free surface were analysed using DFT and the magnitude of the first harmonic was non-dimensionalised with respect to the incident wave amplitude. The pressure on the body was obtained from the numerical solver at the relevant locations for comparison. The comparison is made in figure 16 and it is seen that the agreement can best be described as moderate. Taking the lowest amplitude as the benchmark for comparison, the predictions and measurement agree in terms of general trends but not in terms of values. The reasons for the discrepancies have not yet been ascertained.

7 Discussion and conclusions

This paper provides a comparison of numerical predictions, obtained using a linear hydrodynamic model based upon coefficients calculated using the BEM code WAMIT, and measurements from a dedicated experimental programme; the geometry was a floating vertical circular cylinder. The aim was to investigate the use of a linear hydrodynamic BEM code for this particular geometry and also to establish the limitations of numerical modelling based on linear water wave theory.

The reasonable agreement between the predicted and measured motions of the device gives reasonable confidence in the accuracy of the numerically determined velocity potential. As expected, the agreement is best for the smallest waves and decreases with increasing wave amplitude.

It was established previously that good agreement existed between measured and predicted pressures in the diffraction tests for a fixed cylinder [1]. However, the much poorer agreement between the measured and predicted pressures for the moving cylinder in the present study provides less confidence and is disturbing. Further investigation is clearly needed to establish the causes of the discrepancies, especially as point pressure provides the building blocks for force calculations.

Shortcomings in the linear approach that are probably most prevalent in the present case include viscosity, the evaluation of the boundary condition at the mean body position and the linearisation of the pressure which removes the influence of fluid velocity. Highly nonlinear pressure signals measured in some cases suggest the presence of these physical effects, which are not accommodated by a linear hydrodynamic model.

An assessment of previous and ongoing work on fixed and moving circular moonpools has proved fruitful, with some readily identifiable links established between the two approaches for a similar geometry. It is standard practice in the moonpool community to assume that nonlinearities, due to wave, viscosity or vortex shedding, play an important role in the hydrodynamic behaviour. This is less obvious in the present case, as confirmed by the pressure series, but a detailed parametric study would be required to establish demarcation lines between the differing regimes. This should also be extended to include the influence of energy extraction, the fundamental difference between moonpool and OWC.

At present this work is limited to an undamped OWC as the simpler case must be understood before considering additional external influences which for energy extraction applies some form of free surface damping and hence influences the internal pressures and free surface motion.

In an attempt to examine some of the issues identified above and to assess the usefulness (or otherwise) of the methodology to wider application in the modelling of wave power devices, a smoothed particle hydrodynamics (SPH) code was adapted to study the present and other OWC geometries by Mayrhofer [14]. This study was restricted to a two-dimensional model and the findings were interesting but unfortunately not definitive. The SPH code provided a good model for the LIMPET OWC, predicting the known vortex shedding and nonlinear hydrodynamic behaviour. Unfortunately this was not the case for a fixed vertical OWC, of the type considered herein, as the very small length scales of the OWC relative to the necessarily large fluid domain caused problems. Such codes are computationally very intensive and any attempt at improvement would require considerable resources, so an unresolved discrepancy between prediction and experiment has identified a difficulty with SPH application as well.

Acknowledgements

This research was carried out within the WAVETRAIN Marie Curie Research Training

Network as part of the European Community's FP6 contract MRTN-CT-2003-505166. The authors also would like to thank Garrad Hassan & Partners Ltd. and the Charles Parson Research Initiative for their support during the writing of this paper.

References

[1] Sykes R.K., Lewis A.W. & Thomas G.P. 2007 *A physical and numerical study of a fixed cylindrical OWC of finite wall thickness*. Proc. 7th Eur. Wave & Tidal Energy Conf. Porto, Portugal.

[2] Sykes R.K., Lewis A.W. & Thomas G.P. 2008 *A numerical and physical comparison of a geometrically simple fixed and floating oscillating water column*. Paper OMAE2008-57437, Proc. 27th Int. Conf. on Off. Mech. & Artic Eng., Estoril, Portugal.

[3] Aalbers A.B. 1984 *The water motions in a moonpool*. Ocean Engineering 11(6), 557-579.

[4] Knott G.F. & Flower J. O. 1980 *Measurement of energy losses in oscillatory flow through a pipe exit*. Applied Ocean Research 2, 155-164.

[5] Fung D.P.K. 1996 *Added mass and damping of circular moonpools*. Proc. 6th Int. Conf. on Offshore & Polar Eng., Los Angeles, USA, 247-254.

[6] Sphaier S. H., Torres F.G.S, Masetti I.Q., Costa A.P. & Levi C. 2007 *Monocolumn behavior in waves: Experimental analysis*. Ocean Engineering 34, 1724-1733.

[7] Newman J. N. 1977 *Marine Hydrodynamics* M.I.T. Press.

[8] Newman J. N. 1992 *Panel Methods in Marine Hydrodynamics*. Proc. 11th Australasian Fluid Mechanics Conference, Hobart, Australia.

[9] WAMIT User Manual. www.wamit.com

[10] Isaacson M.St.J 1991 *Measurement of regular wave reflection*. J. Waterway, Port, Coastal and Ocean Engineering, ASCE, 117(6), 553-569.

[11] Payne G.S. 2006 *Numerical modelling of a sloped wave energy device*. PhD thesis, University of Edinburgh.

[12] Lee C.H. 2009 Private communication.

[13] Diebel J. 2006 *Representing attitude: Euler angles, unit quaternions and rotation vectors*. http://ai.stanford.edu/diebel/attitude/attitude.pdf

[14] Mayrhofer A. 2009 *SPHysics in theory and practice*. Final Year Project, University College Cork, Ireland.

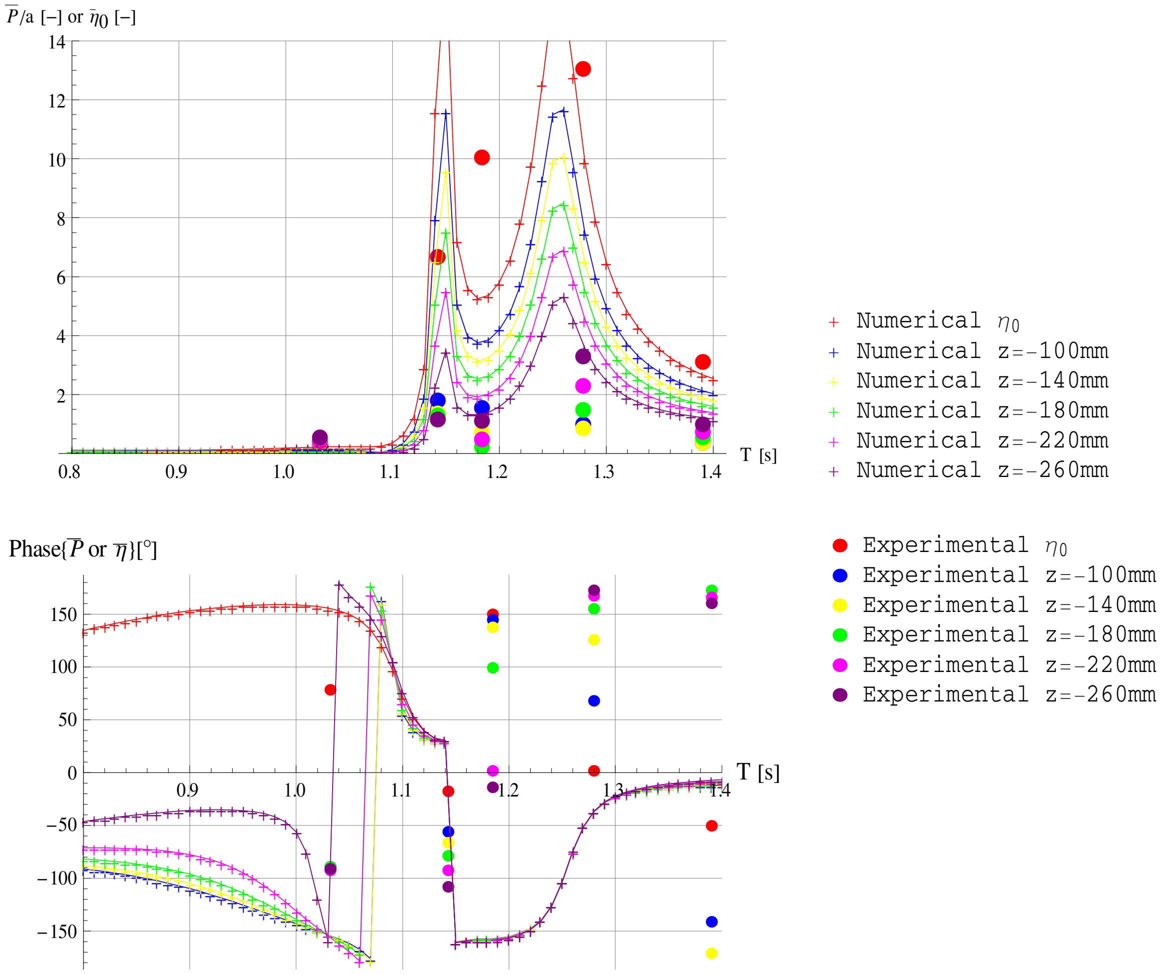

Figure 16: Comparison between numerical and experimental results for water column pressure